Applied Catalysis B: Environmental 138–139 (2013) 362–372

Contents lists available at SciVerse ScienceDirect

Applied Catalysis B: Environmental

journal homepage: www.elsevier.com/locate/apcatb

Cooperative effect of Ce and Mn in $MnCe/Al_2O_3$ environmental catalysts

N. Drenchev, I. Spassova, E. Ivanova, M. Khristova, K. Hadjiivanov*

Institute of General and Inorganic Chemistry, Bulgarian Academy of Sciences, Sofia 1113, Bulgaria

ARTICLE INFO

Article history:
Received 29 December 2012
Received in revised form 4 March 2013
Accepted 6 March 2013
Available online 13 March 2013

Keywords:
Adsorption
CO
NO
FTIR spectroscopy
Catalysis
NO decomposition
Oxidation of CO
NO + CO reaction

ABSTRACT

Three samples, Mn/Al_2O_3, Ce/Al_2O_3 and $MnCe/Al_2O_3$ (containing 10 wt.% metal) were prepared by impregnation and comparatively studied by means of FTIR spectroscopy, other characterization techniques and catalytic measurements. It was established that the active phase deposition led to (i) partial disappearance of all kinds of the alumina OH groups and (ii) blocking of part of the Al^{3+} Lewis acid sites. The results indicated that manganese was better dispersed on the $MnCe/Al_2O_3$ sample as compared to Mn/Al_2O_3. As a result, the bimetallic sample was the most active one in a series of catalytic reactions: NO decomposition, CO oxidation and CO + NO interaction.

Interaction of all samples with CO leads to formation of carbonates and hydrogencarbonates increasing in amount with the temperature of interaction and in the sequence $Al_2O_3 < Ce/Al_2O_3 < Mn/Al_2O_3 \ll MnCe/Al_2O_3$. When the samples interacted with NO, different nitrogen oxo-compounds were formed and manganese nitrosyls appeared with the Mn-containing samples. In agreement with the higher Mn dispersion, the amount of the latter was larger with the bimetallic sample. Interaction between CO and NO results in formation of isocyanates, (hydrogen)carbonates and nitrogen oxo-compounds (nitrosyls, nitro-nitrito and nitrate species). When the interaction occurs at ambient temperature, the surfaces of the Al_2O_3, Ce/Al_2O_3 and Mn/Al_2O_3 are covered mainly by nitrates and nitro-nitrito species. With increase of the interaction temperature these species are gradually replaced by (hydrogen)carbonates. The temperature of this replacement decreases in the order Al_2O_3–Ce/Al_2O_3–Mn/Al_2O_3. With the $MnCe/Al_2O_3$ sample carbonates dominate even at 373 K interaction. Consequently, the NO + CO catalytic conversion occurs in two regimes. The low temperature regime (the temperature interval depends on the catalyst) is associated with NO_x precovered surface, while at higher temperatures the catalysts surfaces are precovered with (hydrogen)carbonates.

1. Introduction

Environmental concerns have stimulated many efforts on the development of efficient catalytic methods for control of harmful compounds evolved by stationery and mobile sources. Special attention has been paid to the full oxidation of CO and hydrocarbons and to reduction of NO_x in exhaust gases. Especially for reduction of NO_x emission, different approaches have been proposed. Among them the direct NO decomposition, storage-reduction and selective catalytic reduction are considered to be prospective routes [1–4].

Although many chemical and mechanistic studies about CO oxidation [5–7] and NO_x reduction were performed [1,8–10], important details on reaction mechanisms are still under debate. Consequently, the design of effective catalysts for environmental protection is still rather an art. Many systems have been studied by varying the components of the active phases, the supports and the preparation conditions. Precious metals, single and composite oxides, etc. have been investigated in order to find efficient, cheap and usable catalysts for environmental purposes. Recently, ceria based catalysts with addition of transition metal(s) have attracted much attention [4,11–13]. These catalysts are good candidates for NO_x and CO elimination processes because of the pronounced redox properties of ceria and its strong interaction with transition metals [14–16].

In a recent paper some of us have studied a series of alumina-supported catalysts containing Ce and/or Mn with various ratios as active phase [17]. It was established that alumina supported mixed ceria–manganese catalysts have a potential in methanol decomposition and in an integrated process for NO reduction with methanol decomposition products. The best catalytic performance in the CO–NO reaction was achieved with a $MnCe/Al_2O_3$ sample with a 1:1 ratio between Mn and Ce. In order to obtain a deeper insight into reaction mechanism, we performed a detailed FTIR mechanistic study on this reaction using three catalysts: the most

* Corresponding author. Tel.: +359 29793598; fax: +359 28705024.
E-mail address: kih@svr.igic.bas.bg (K. Hadjiivanov).

0926-3373/$ – see front matter © 2013 Elsevier B.V. All rights reserved.
http://dx.doi.org/10.1016/j.apcatb.2013.03.012

active $MnCe/Al_2O_3$ sample (1:1 molar ratio) and two monometallic (Ce/Al_2O_3 and Mn/Al_2O_3) samples. The results were compared with the catalytic performance of the samples in the CO oxidation, NO decomposition and CO + NO reaction.

2. Experimental

2.1. Samples

The parent γ-Al_2O_3 sample was a commercial alumina (Alfa Aesar) with a specific surface area of 250 $m^2\,g^{-1}$ and pore volume (V_t) of 1 $cm^3\,g^{-1}$. A fraction of this sample between 0.3 and 0.8 mm was used for the catalytic tests and for preparation of the catalysts.

The Mn- and Ce-containing catalysts were prepared by impregnation of the support at 333 K with solutions of the respective nitrate salts (0.034 g ml^{-1} Mn and 0.036 g ml^{-1} Ce for monometallic samples and 0.025 g ml^{-1} Mn and 0.025 g ml^{-1} Ce for the bimetallic sample). The procedure was carried out after preliminary evacuation of the support at a residual pressure of 3.33 kPa and then the liquid phase was evaporation under the same pressure. The nominal total metal (Ce, Mn) concentration in the samples was chosen to be 10 wt.% (5 wt.% for each metal in the $MnCe/Al_2O_3$ sample).

2.2. Techniques

FTIR spectra were recorded with a Nicolet 6700 spectrometer accumulating 128 scans at a spectral resolution of 2 cm^{-1}. Self-supporting pellets (ca. 10 mg cm^{-2}) were prepared from the powdered samples and treated directly in a purpose-made IR cell allowing measurements at ambient and low temperature (100 K). The cell was connected to a vacuum-adsorption apparatus with a residual pressure below 10^{-3} Pa. Prior to the adsorption experiments, the samples were activated by calcinations at 673 K for 1 h and evacuation at the same temperature for 1 h.

The DR UV-Vis spectra were recorded using a Thermo Scientific Evolution 300 UV-Vis spectrophotometer equipped with a diffuse reflectance unit.

Catalytic activity tests of CO oxidation and NO decomposition were performed using an integrated quartz micro-reactor and mass spectrometer system (CATLAB, Hiden Analytical, UK). The system features a fast-response, low thermal mass furnace with integrated air-cooling, a precision Quadrupole Mass Spectrometer, and a quartz inert capillary with "hot zone" inlet for continuous close-coupled catalyst sampling with minimal dead volume and memory effects. The reactant gases were supplied through electronic mass flow controllers. The catalysts (400 mg grains with particles size of 0.3–0.8 mm) were held between plugs of quartz wool in a quartz tubular vertical flow reactor (Ø = 6 mm). Before the measurements the catalysts were pretreated under Ar flow at 773 K (ramp temperature of 10 K min^{-1}) and then the reactor was cooled down to ambient temperature. The CO oxidation or NO decomposition tests were performed from 313 K to 773 K, with a gas mixtures of Ar:CO:O_2 (98.5:0.5:1 vol.%) and Ar:NO (99.5:0.5 vol.%) kept at a constant flow of 400 $cm^3\,min^{-1}$. The mixtures also contained about 150 ppm residual water. During the catalytic and desorption tests, the following arbitrary mass units (amu) [m/e] have been collected simultaneously by the Quadrupole Mass Spectrometer: 2 (H_2), 18 (H_2O), 28 (CO), 32 (O_2), 40 (Ar), and 44 (CO_2) – for the CO oxidation and 28 (N_2), 30 (NO), 32 (O_2), 40 (Ar), 44 (N_2O), and 46 (NO_2) – for NO decomposition. The contributions due to N_2O cracking fragments (m/e = 28 and 30) have been subtracted when measuring N_2 and NO.

The reduction of NO with CO was carried out in a conventional flow apparatus from 298 K to 773 K with an isothermal flow quartz reactor with a gas mixture containing Ar:NO:CO (99.5:0.25:0.25 vol.%) at a constant flow of 400 $cm^3\,min^{-1}$. The inlet and outlet concentrations of NO, CO, and CO_2 were controlled by infrared gas analyzers. N_2O was measured spectrophotometrically, and a thermal converter was used for the total analysis of NO_x ($NO + NO_2$). The specific activity (SA) values were calculated as amount of CO (NO) converted per unit metal content for 1 h.

3. Results and discussion

3.1. Initial characterization of the samples

Some characteristics of the samples investigated are presented in Table 1.

The basic characterization of the samples by XRD, TPR, XPS and low temperature nitrogen adsorption was already reported [17]. Briefly, it was established that Mn_2O_3 and CeO_2 existed on the Mn/Al_2O_3 and Ce/Al_2O_3 samples, respectively. The $MnCe/Al_2O_3$ catalyst contained $MnO_{1.88}$, Mn_2O_3, CeO_2 and $CeAl_{11}O_{18}$ phases. However, only CeO_2 was detected by XRD which indicates that the Mn-containing phases were highly dispersed. This was confirmed by the TEM results.

The DR UV-Vis spectra of the samples are presented in Fig. S1 from the Supplementary Content. Alumina has practically no absorbance in the 200–1100 nm region. The Ce/Al_2O_3 sample shows a main peak at 295 nm, typical of supported CeO_2 nanoparticles [18,19]. A shoulder at 255 nm could suggest presence of some Ce^{3+} sites ($Ce^{3+} \leftarrow O^{2-}$ LMCT) [18]. The Mn/Al_2O_3 sample is characterized by a complex spectrum where an intense band at 350 nm dominates. In addition, a band at 260 nm and a broad absorbance at higher wavelengths are well discernible. The latter has an ill-resolved maximum around 500 nm. According to data from the literature [20] the main band at 350 nm indicates the presence of Mn^{3+} cation. This is consistent with the XRD and TEM data evidencing existence of Mn_2O_3 particles. The continuous absorption in the visible region can also be related to the d–d transfer of Mn^{3+}. However, the feature around 500 nm suggests existence of some Mn^{4+} ions [20], possibly on the surface of the Mn_2O_3 particles. Finally, the band at 260 nm is to be assigned to Mn^{2+} ions in tetrahedral coordination [21]. The latter species should be highly dispersed, because no separate Mn^{2+}-containing phase was detected by XRD and SAED.

The spectrum of the $MnCe/Al_2O_3$ sample contains a feature at 288 nm which can be attributed to CeO_2 nanoparticles. The small difference of the peak maximum as compared with the Ce/Al_2O_3 sample is probably due to the coexistence of manganese. The most intense band is at 255 nm, already associated with Mn^{2+} ions. However, some contribution of Ce^{3+} sites is not excluded [18]. At the same time, the bands indicative of the presence of Mn^{3+} and/or Mn^{4+} ions appear only as shoulders, which implies a low amount

Table 1
Some characteristics of the samples studied [17].

Sample	Mn and/or Ce (mass %)	S_{BET} ($m^2\,g^{-1}$)	Phase composition, XRD	Phase composition, TEM (SAED)
Al_2O_3	–	250	γ-Al_2O_3	γ-Al_2O_3
Ce/Al_2O_3	9.9	193	CeO_2, γ-Al_2O_3	CeO_2, γ-A_2O_3
Mn/Al_2O_3	10.1	191	Mn_2O_3, γ-Al_2O_3	Mn_2O_3, γ-Al_2O_3
$MnCe/Al_2O_3$	5.2/4.9	194	CeO_2, γ-Al_2O_3	$MnO_{1.88}$, Mn_2O_3, CeO_2, $CeAl_{11}O_{18}$, γ-Al_2O_3

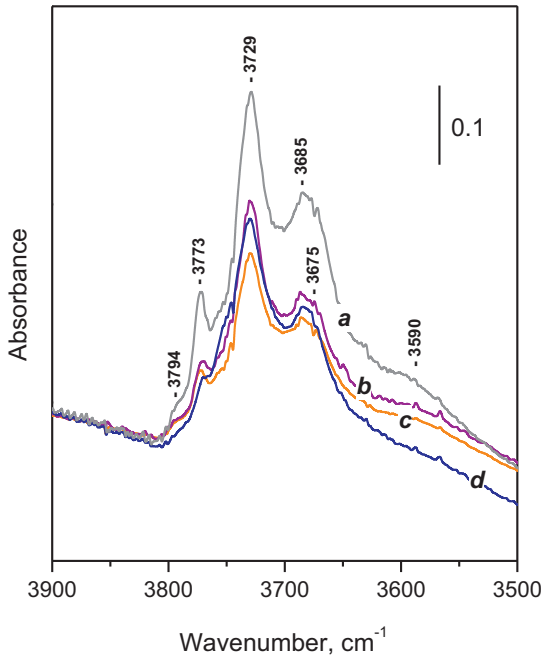

Fig. 1. FTIR spectra in the OH stretching region of the activated Al_2O_3 (a), Mn/Al_2O_3 (b), Ce/Al_2O_3 (c) and $MnCe/Al_2O_3$ (d).

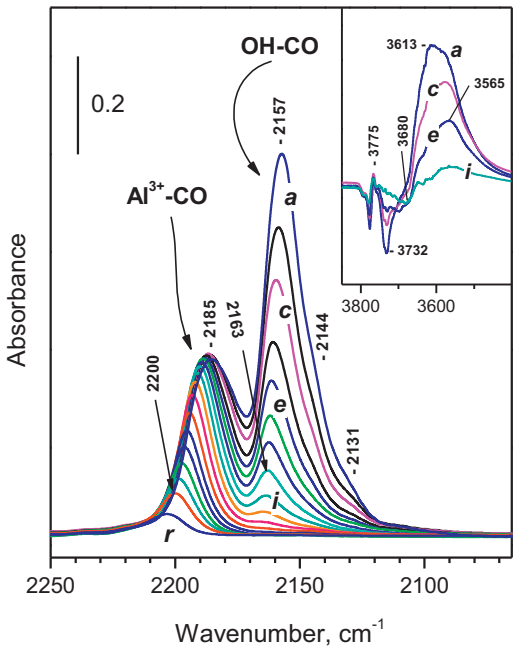

Fig. 2. FTIR spectra (carbonyl region) of CO adsorbed at 100 K on the Al_2O_3 support. Equilibrium CO pressure of 200 (a), 100 (b) and 50 Pa (c) and evolution of the spectra during evacuation (d–r). The inset shows the changes in the OH stretching region. The spectra are background and CO gas-phase corrected.

of Mn_2O_3. Indeed, this compound was not registered in the XRD spectra of the sample. Therefore, the UV–vis spectra lead to the conclusion that addition of cerium results in substantial increase of manganese dispersion and, at the same time, keeps manganese in a low oxidation state.

3.2. FTIR results

3.2.1. Background FTIR spectra of the activated samples

The background spectrum of the activated parent Al_2O_3 material contains, in the OH stretching region, four well resolved bands with maxima at 3794, 3773, 3729 and 3685 cm^{-1} (Fig. 1, spectrum a). A broad band around 3590 cm^{-1} is also distinguished. The spectrum is typical of γ-alumina and, according to Knözinger and Ratnasamy [22] and other authors [23–29], the band at 3794 and 3773 cm^{-1} are due to OH groups in octahedral and tetrahedral coordination, respectively. These OH groups are of type I, i.e. connected to one Al atom each. The band at 3729 cm^{-1} is attributed to hydroxyl groups bonded to two aluminum atoms (type II), one of which is in tetrahedral, and the other in octahedral coordination. The band at 3680 cm^{-1} is assigned to OH groups bonded to three aluminum atoms in octahedral coordination [22–29]. Finally, the band at 3590 cm^{-1} characterizes H-bonded hydroxyls.

Three very weak bands, at 1570, 1472 and 1374 cm^{-1} are assigned to residual carbonate-like structures [30–33]. These bands appeared with similar intensity in the spectra of Mn- or/and Ce-containing samples. The spectra also indicate the absence of sulfates (characterized by a strong band around 1380 cm^{-1} [34]) that can strongly affect the surface properties of oxides.

The spectra of all supported materials are similar to that of the support (Fig. 1, spectra b and c). However, the OH bands appeared with a reduced intensity. We will emphasize that:

- The highest frequency hydroxyls (3773 cm^{-1}) and the H-bonded hydroxyls are most affected with the $Mn–Ce/Al_2O_3$ sample.
- The band at 3729 cm^{-1} is slightly more affected with the Ce/Al_2O_3 sample as compared with the other two supported materials.

These results indicate that during the deposition of the active phase part of the OH groups of the support have reacted with the supported species. However, this interaction is restricted and non-selective. The H-bonded hydroxyls are the only exception because they seem to be almost fully consumed with the $MnCe/Al_2O_3$ sample.

3.2.2. Interaction of the samples with CO

Species supported on oxides, in particular alumina, can be located at (i) the places where the OH groups of the support have initially existed and/or (ii) Lewis acid-basic pairs. While the former location can be easily monitored by the background spectra of the materials in the OH stretching region, for the establishment of location on acid-basic pairs probe molecules should be applied. Briefly, in this case the Lewis acid sites of the support are blocked [35]. One of the most convenient probe molecules for establishing the location of supported species is CO. However, the adsorption should be performed at low temperature in order to detect even the weakest acid sites.

The first step of this characterization was to study the interaction of CO with the support at low temperature. The FTIR spectra of CO adsorbed at 100 K on the parent Al_2O_3 material are presented in Fig. 2. Introduction of CO to the sample results in the appearance of two principal bands located at 2185 and 2157 cm^{-1} (Fig. 2, spectrum a). Two shoulders (physically adsorbed CO) are also visible at 2144 and 2131 cm^{-1}. Simultaneously, the OH groups decrease in intensity and a new broad band at lower frequencies develops. The latter has distinguished maxima at 3613 and 3565 cm^{-1} (see the inset in Fig. 2, spectrum a). Decrease of the equilibrium CO pressure and further evacuation lead to decrease in intensity of the 2157 cm^{-1} band until its disappearance. At low coverages the maximum is shifted to 2163 cm^{-1} (Fig. 2, spectra f–j). In parallel with these changes the broad OH band also disappears and the initial OH spectrum is gradually restored (see the inset in Fig. 2). A careful analysis of the spectra indicates that the OH band around 3732 cm^{-1} is shifted to 3618 cm^{-1} ($\Delta\nu = 114\ cm^{-1}$) and a carbonyl band at 2157 cm^{-1} is associated with this shift. The band around

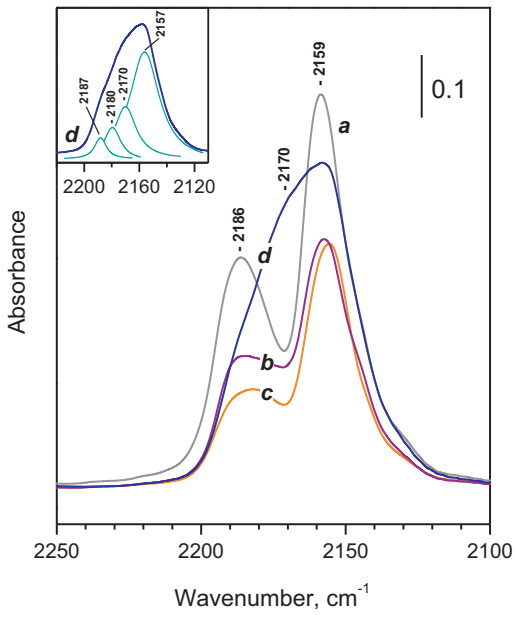

Fig. 3. FTIR spectra of CO (100 Pa equilibrium pressure) adsorbed at 100 K on the activated Al_2O_3 (a), Mn/Al_2O_3 (b), Ce/Al_2O_3 (c) and $MnCe/Al_2O_3$ (d). The inset shows computer deconvolution of spectrum d. The spectra are background and CO gas-phase corrected.

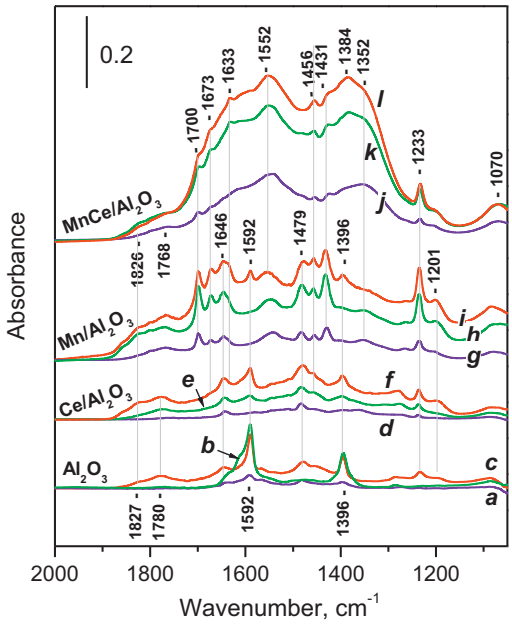

Fig. 4. FTIR spectra of the surface species produced after interaction of the samples with CO (1 kPa pressure, 10 min) at different temperatures. Samples: Al_2O_3 (a–c); Ce/Al_2O_3 (d–f), Mn/Al_2O_3 (g–i) and $MnCe/Al_2O_3$ (j–l); temperatures: 473 K (a, d, g and j), 573 K (b, e, h and k) and 673 K (c, f, i and l). The spectra are background corrected.

3680 cm^{-1} is shifted to 3560 cm^{-1} ($\Delta\nu$ = 120 cm^{-1}). Although the shift is similar, the spectra clearly indicate that the carbonyl complexes of the 3680 cm^{-1} OH groups are more stable because are observed at lower CO coverages. In addition, the corresponding carbonyl band is detected at 2163 cm^{-1} which suggests a higher acidity of the hydroxyl groups. All these results impeach the use of $\Delta\nu$(OH) as a correct measure for the hydroxyl acidity, especially in the cases when they strongly differ in stretching frequency.

Comparison with available literature data shows that the CO-induced shifts we have measured are slightly larger than those reported by Zaki and Knözinger (70–95 cm^{-1}) [36] and Soltanov et al. (100 cm^{-1}) [37] but slightly smaller than measured by El-Nadjar et al. (145 cm^{-1}) [26].

Finally, it appears that the 3775 cm^{-1} hydroxyls are also affected upon CO adsorption. This is opposite to some reports, claiming this band is not affected by CO [25,36], but in agreement with recent observations [26]. The higher frequency component at 3795 cm^{-1} is affected at very low coverages and could be associated with CO adsorbed on the Lewis acid sites. The band at 3775 cm^{-1} is continuously affected at all CO coverages. Based on our results, it is difficult to establish the exact CO-induced shift of the O—H stretchings of these hydroxyls.

The spectra of CO adsorbed at 100 K and 100 Pa equilibrium pressure on all samples are compared in Fig. 3. The results obtained with Ce/Al_2O_3 and Mn/Al_2O_3 are very similar. In both cases the band at 2159 cm^{-1} (already assigned to OH–CO interaction) appeared with reduced intensity which is consistent with the lower hydroxyl coverage on these samples as compared to the support. Also the band at 2186 cm^{-1} was reduced in intensity which indicates that some c.u.s. Al^{3+} sites have been blocked after the deposition of the active phase. Lower frequency components of the 2186 cm^{-1} band (observed with both samples around 2180 cm^{-1} and at ca. 2175 cm^{-1} for Mn/Al_2O_3) can be attributed to CO interacting with Mn^{n+} or Ce^{n+} sites [33].

The spectrum of CO adsorbed on the $MnCe/Al_2O_3$ sample is different. A halo centered on 2170 cm^{-1} is indicative of CO interaction with Mn and/or Ce cations and evidences a high dispersion of at least one of the components of the supported phase. Computer deconvolution suggests two bands with maxima at 2180 and 2170 cm^{-1} (see the inset in Fig. 3). The intensity of the band due to OH–CO complexes is similar for all supported samples, while the intensity of the band at 2186 cm^{-1} (Al^{3+}–CO) is slightly lower with the $MnCe/Al_2O_3$ sample.

In order to obtain more information on the nature of the different carbonyl species we have studied CO adsorption on different coverages. The details are presented in the Supplementary Content (Figs. S2–S4) and the main conclusions that can be drawn are:

- Two bands, at 2181 and 2175 cm^{-1} are distinguished at low coverage in the spectra of CO adsorbed on the Ce/Al_2O_3 sample. These bands are assigned to Ce^{n+}-CO species.
- A shoulder around 2176 cm^{-1} (Mn^{n+}-CO) is detected at low coverages with the Mn/Al_2O_3 sample.
- An intense band at 2168 cm^{-1} is well observed with the $MnCe/Al_2O_3$ sample. This carbonyl band shifts to 2184 cm^{-1} at low coverage. Such a shift, called chemical shift, is indication for a close packing of the adsorbed molecules. Thus, the results indicate that the CO adsorption sites are not isolated cationic species but form separate two- or three-dimensional phases. We assign these carbonyls to Mn^{2+}–CO species [33]. Note that similar species could contribute to the band at 2187–2193 cm^{-1} assigned to Al^{3+}–CO complexes [33].
- No carbonate-like structures are formed at the experimental conditions applied.

The next step in the CO adsorption experiment was to check the reactivity of the alumina and the supported phases towards CO. For that purpose the samples were heated in CO atmosphere at different temperatures and then cooled again to ambient temperature. The spectra registered after interaction of the samples with CO at 473, 573 and 673 K are presented in Fig. 4. Because of the appearance of too many bands their assignments are summarized in Table 2.

Two kinds of species, carbonates and hydrogencarbonates were registered on the different samples. A band around 1220 cm^{-1},

Table 2
Assignment of the carbonate-like surface species observed after interaction of CO with the samples and temperature of their appearance [30,32].

Set of bands (cm^{-1})	Al_2O_3	Ce/Al_2O_3	Mn/Al_2O_3	$MnCe/Al_2O_3$	Assignment
1646–1633; 1479; 1233	+ at 673 K	+ at 473 K	+ at 473 K	+ at 473 K	Hydrogencarbonates I type [30,32]
1673; 1456; 1233	+ at 673 K	+ at 473 K	+ at 473 K	+ at 473 K	Hydrogencarbonates II type [30,32]
1700; 1431; 1233	–	–	+ at 473 K	+ at 473 K	Hydrogencarbonates III type [30,32]
1826–1768; 1201	+ at 673 K	+ at 573	+ at 474 K	+ at 474 K	Bridged carbonates [30,32]
1592; 1396	+ at 473 K	+ at 573 K	+ at 673 K		Tricoordinated carbonates I type [30,32]
1552; 1384–1352	–	–	+ at 473 K	+ at 473 K	Tricoordinated carbonates II type [30,32]

due to δ(C—O···H) modes is characteristic of hydrogencarbonates [30]. The respective ν_{as}(COO) and ν_s(COO) modes are observed around 1650 and 1440 cm^{-1}, respectively, and are highly sensitive to the way of coordination. With our samples they are registered in the 1700–1633 and 1479–1431 cm^{-1}, respectively. In addition, the ν(OH) modes with all samples appeared between 3608 and 3616 cm^{-1}.

The free carbonate ion is characterized by an IR active $\nu_{as}(CO_3)$ mode at 1450–1420 cm^{-1} and an IR silent $\nu_s(CO_3)$ vibration at 1090–1020 cm^{-1} [38]. The latter can be observed in the IR spectra only after symmetry reduction. As a general rule, the $\nu_{as}(CO_3)$ mode is split during adsorption and this split is larger for bridged carbonates, smaller for bidentate ones and even smaller for mono- or tridentate carbonates. Therefore, we assign the band in the 1826–1768 cm^{-1} region, together with bands around 1200 cm^{-1}, to bridged carbonates. It has recently been pointed out that the probability of formation of monodentate carbonates on the surfaces is small [39] and we prefer to assign the bands at 1592–1552 and 1396–1352 cm^{-1} to tridentate carbonates.

Bands around 1070 cm^{-1} could be due to carbonates or hydrogencarbonates and seems to be not specific. For that reason these bands will be not discussed further on.

Analysis of Fig. 4 shows that alumina support possesses the weakest reactivity towards CO. At 473 K only small amount of carbonates (1592 and 1396 cm^{-1}) are formed and their amount increases when the interaction temperature is 573 K (Fig. 4, spectra a and b). At 673 K bridging carbonates (1826–1768 and 1201 cm^{-1}) and hydrogencarbonates (1646, 1479 and 1233 cm^{-1}) are formed (Fig. 4, spectrum c). A closer inspection of the spectra indicates a second type of hydrogencarbonates (1673, 1456 and 1233 cm^{-1}) in low concentration. Note that the band at 1233 cm^{-1} is slightly sensitive to the coordination and may characterize different hydrogencarbonate species.

Interaction of CO with the Ce/Al_2O_3 sample results in a similar picture (Fig. 4, spectra d–f). In this case, however, the formation of carbonates characterized by bands at 1592 and 1396 cm^{-1} is slightly hindered. This could be associated with lower alumina surface exposed on the sample, as compared to the support. On the contrary, the other bands are slightly more intense which can be explained by the ability of ceria to provide reactive oxygen.

The spectra recorded after interaction of CO with the Mn/Al_2O_3 sample are more complicated (Fig. 4, spectra g–i). At first, the hydrogencarbonates characterized by bands at 1673 and 1456 cm^{-1} appear with enhanced intensity. Several bands, at 1700, 1552, 1431 and 1352 cm^{-1} have not been recorded with the Mn-free samples. The bands at 1700 and 1431 cm^{-1} are attributed to another kind of hydrogencarbonates probably coordinated to manganese ions. The bands at 1552 and 1352 cm^{-1} are assigned to tricoordinated carbonates, again probably connected to Mn ions. Another type of bidentate carbonates, characterized by a band at 1768 cm^{-1}, was also registered.

The amount of carbonate structures is highest with the $MnCe/Al_2O_3$ sample. Two bands at 1552 and 1384 cm^{-1} (assigned to tridentate carbonates) dominate in the spectra. These species can be associated with the manganese content.

The most important conclusions that can be made are:

- With all samples the amount of carbonate-like structures increases with the temperature of interaction.
- The concentration of carbonate-like structures is lowest with the Al_2O_3 sample and increases in the order $Ce/Al_2O_3 < Mn/Al_2O_3 \ll MnCe/Al_2O_3$.

3.2.3. Interaction of the samples with NO

Nitrogen monoxide is another widely applied probe molecule, often giving information supplementary than that obtained with CO [40]. The electrostatic bonding is not typical of this probe and, as a result, it does not interact (or interacts weakly) with typical electrostatic Lewis acids, as Al^{3+}, Ti^{4+}, Zr^{4+}, Ce^{4+}, etc. In contrast, NO forms stable mono- and dinitrosyls with other cations, as Cu^{2+}, Mn^{n+}, Co^{2+}, etc.

The spectra of NO (1 kPa equilibrium pressure) adsorbed on the different samples are compared in Fig. 5 and the assignments of the bands observed are summarized in Table 3.

The most intense band formed on Al_2O_3 is at 1225 cm^{-1} (Fig. 5, spectrum a). This band has already been observed on alumina and, together with a band at 1324 cm^{-1}, is assigned to nitro-nitrito species. Two other bands, at 1467 and 1079 cm^{-1}, are also assigned to similar species. A weak band at 2534 cm^{-1} (not shown) is attributed to combination modes [41]. It was reported that all these bands easily disappear in the presence of oxygen because of conversion of the respective species to nitrates [27]. A weak band at 1611 cm^{-1} is due to nitrates [40], the respective low frequency counterparts being probably masked by the intense band at 1225 cm^{-1}.

The spectra of NO adsorbed on Ce/Al_2O_3 are similar to those registered with alumina, but most of the bands were more intense (Fig. 5, spectrum b). Weak additional features at 1642 cm^{-1} (nitrates) and 1358 cm^{-1} (nitrites) are also distinguished. Two

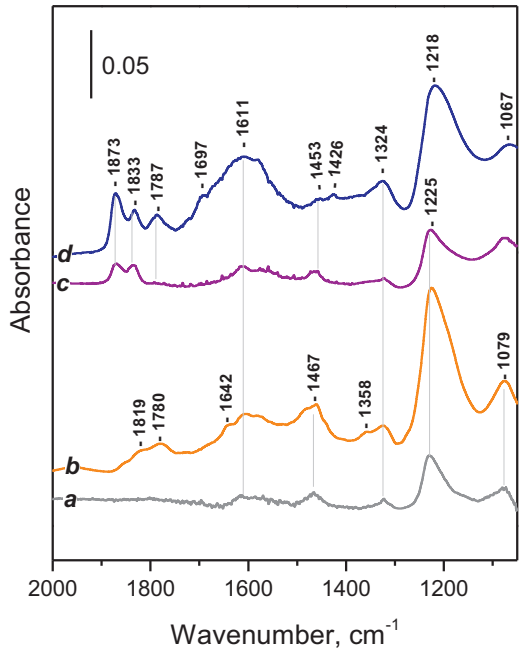

Fig. 5. FTIR spectra of the surface species produced after adsorption of NO (1 kPa equilibrium pressure, 298 K) on Al_2O_3 (a) Ce/Al_2O_3 (b), Mn/Al_2O_3 (c) and $MnCe/Al_2O_3$ (d). The spectra are background and gas-phase corrected.

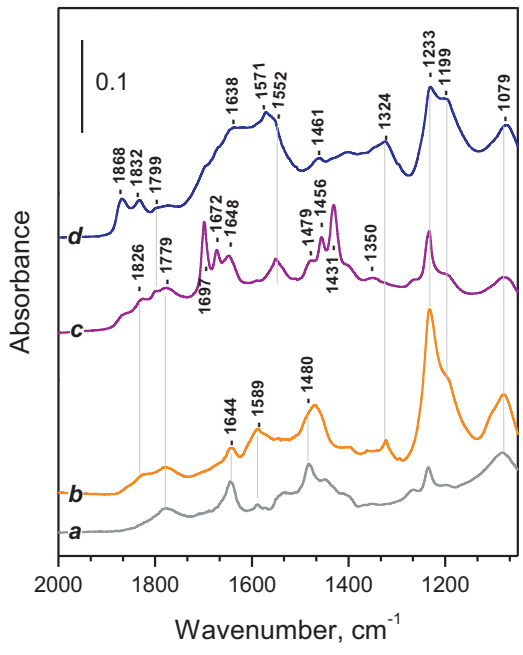

Fig. 6. FTIR spectra of the surface species produced after interaction of NO (1 kPa equilibrium pressure, 673 K) with Al_2O_3 (a) Ce/Al_2O_3 (b), Mn/Al_2O_3 (c) and $MnCe/Al_2O_3$ (d). The spectra are background and gas-phase corrected.

bands, at 1819 and 1780 cm^{-1} are likely due to N_2O_3. The results indicate that ceria additives slightly affect the way of NO adsorption on alumina mainly by providing reactive oxygen for NO oxidation.

The spectrum of NO adsorbed on Mn/Al_2O_3 was also similar to that observed with the pure support (Fig. 5, spectrum c). However, three bands at 1873, 1833 and 1787 cm^{-1} are additionally registered. These bands are assigned to nitrosyls of manganese sites [42–44]. There is no consensus in the literature about the oxidation state of manganese in the different surface nitrosyl complexes. Thus, according to Kapteijn et al. [42], bands at 1865 and 1833 cm^{-1}, observed with Mn/Al_2O_3, are due to Mn^{3+}–NO complexes. Kantcheva attributed bands at 1905, 1880–1870 and 1865 cm^{-1} (appearing after NO adsorption on Mn/TiO_2) to Mn^{3+}–NO species and a band at 1798 cm^{-1}, to Mn^{2+}–NO species [43]. According to Bell et al. [44], the Mn^{2+}–NO species in Mn-ZSM-5 are observed at 1894 cm^{-1}, while the Mn^{3+}–NO species absorb in the 1966–1935 cm^{-1} region. Taking into account the CO adsorption results, we assign the bands at 1873, 1833 and 1787 cm^{-1} to nitrosyls of Mn^{2+}.

The bands assigned to Mn^{2+}–NO species were more intense with the $MnCe/Al_2O_3$ sample which is consistent with the higher manganese dispersion and lower average oxidation state. Also, the amount of nitrates characterized by a band at 1611 cm^{-1} was much more important with this sample.

The next step was to follow the interaction of the samples with NO at different temperatures. As in the case of interaction with CO, the amount of the surface species formed increased with temperature. Fig. 6 compares the spectra obtained after the interaction of the different samples with NO at 673 K. Details on the interaction at intermediate temperatures are provided in the Supplementary Content (Figs. S5–S8).

The amount of surface species formed on alumina after interaction with NO significantly increases when rising the temperature to 673 K. A band at 1779 cm^{-1} is assigned to N_2O_3. Nitrates (1644 cm^{-1}) and nitrites (1480 cm^{-1}) are the main additional products. Similar situation was observed with the Ce/Al_2O_3 sample.

Surprisingly, in the spectra observed after interaction of NO with Mn/Al_2O_3 sample at 673 K, bands typical of hydrogencarbonates (1697, 1672, 1648, 1479, 1456 and 1421 cm^{-1}) were observed. These results suggest that surface carbon species non-visible by IR have existed on the surface prior to NO adsorption. Evidently, they have resisted oxidation with oxygen during the sample activation. In order to check the validity of this hypothesis, we treated the sample several ways with NO. The amount of hydrogencarbonates gradually decreased and they were not observed after four NO adsorption–desorption cycles. Additional experiments with subsequent CO adsorption, followed by NO adsorption, revealed that such carbon was not produced as a result of CO dissociation.

Finally, NO interaction with the $MnCe/Al_2O_3$ sample at 673 K led mainly to additional formation of nitrates, characterized by bands at 1571 and 1233 cm^{-1}. However, small amount of hydrogencarbonates (much less as compared to the Mn/Al_2O_3 sample) were observed with this sample as well. The respective carbon species

Table 3
Assignment of the NO_x surface species observed after interaction of NO with the samples [40].

Set of bands	Al_2O_3	Ce/Al_2O_3	Mn/Al_2O_3	$MnCe/Al_2O_3$	Assignment
1873, 1833 and 1787 cm^{-1}	–	–	+	+	Mn^{2+}–NO
1819 and 1780 cm^{-1}	+	+			N_2O_3
1225 + 1324 and 2534 cm^{-1}	+	+	+	+	Nitro-nitrito species
1076 cm^{-1}	+	+			Nitro-nitrito species
1467 cm^{-1}	+	+			Nitro-nitrito species
1644 and 1611 cm^{-1}	+	+			Nitrates
1453 and 1426 cm^{-1}	–	–	+	+	Nitro

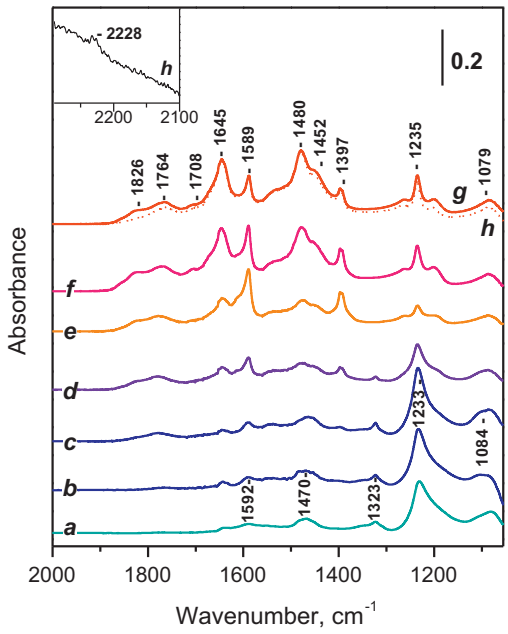

Fig. 7. FTIR spectra of the surface species produced after interaction of NO and CO (1 kPa initial equilibrium pressure of each gas) with Al_2O_3. Temperature of interaction 373 (a), 423 (b), 473 (c), 523 (d), 573 (e), 623 (f) and 673 K (g) and after evacuation (h). The spectra are background and gas-phase corrected.

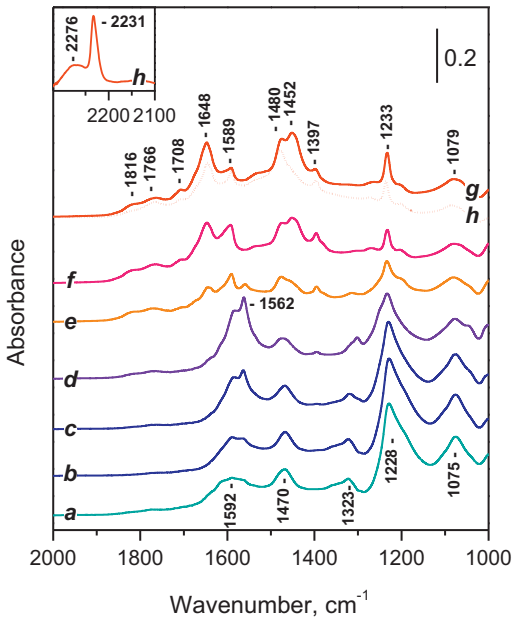

Fig. 8. FTIR spectra of the surface species produced after interaction of NO and CO (1 kPa initial equilibrium pressure of each gas) with Ce/Al_2O_3. Temperature of interaction 373 (a), 423 (b), 473 (c), 523 (d), 573 (e), 623 (f) and 673 K (g) and after evacuation (h). The spectra are background and gas-phase corrected.

can be associated with manganese content, but evidently, addition of ceria leads to a strong decrease in their amount.

3.2.4. Coadsorption of CO and NO (IR mechanistic studies)

In order to obtain information on the interaction between CO and NO on the samples, we have studied the coadsorption of the two gases at different temperatures.

The spectra registered after CO + NO interaction of alumina are presented in Fig. 7. At low temperature (373 K) the products are essentially the same as those obtained after adsorption of pure NO. With increase of the interaction temperature products assigned to carbonate-like structures are formed (bands at 1826, 1764, 1708, 1645, 1589, 1480, 1452, 1397, 1235, 1079, see Table 1 for the assignments). These products start to appear at 473 K and at 573 K practically no NO_x compounds were observed on the surface. Analysis of the region between 2300 and 2100 cm^{-1} shows that only a very weak band at 2231 cm^{-1} was recorded. This band is assigned to Al–NCO species [45] and we emphasize that the latter are in a very low concentration. A band of negligible intensity at 2347 cm^{-1} was also detected and assigned to adsorbed CO_2 (see Fig. S9 from the Supplementary Content).

The picture is similar with the Ce/Al_2O_3 sample. At low temperatures nitrogen-oxo species dominate on the surface and are gradually replaced by carbonate-like structures with the temperature increase (Fig. 8). Note that this replacement occurs at lower temperature as compared to the pure Al_2O_3 sample. In this case two bands, at 2276 and 2231 cm^{-1} are well discernible in the 2300–2100 cm^{-1} region. These two bands were also observed with the Mn/Al_2O_3 sample (see below) and are assigned to isocyanates (NCO^-) attached to aluminum sites. Some amount of adsorbed CO_2 was also monitored by a band at 2347 cm^{-1} (see Fig. S9 from the Supplementary Content). The band increased in intensity with the increase of the interaction temperature and disappeared after evacuation.

The same trends are observed with the Mn/Al_2O_3 sample (Fig. 9). Here again, at low temperatures, nitrogen-oxo species prevail on the surface. Their replacing with carbonate-like structures occurs at definitely lower temperatures as compared to the alumina and Ce/Al_2O_3 samples. In this case the isocyanate bands at 2276 and 2231 cm^{-1} have also been produced. In addition, a weak band at 2253 cm^{-1} is also recorded and associated with isocyanates on manganese sites. As for the CO_2 band (registered at 2345 cm^{-1}), it was of comparable intensity with that registered with the Ce/Al_2O_3 sample.

The spectra registered after CO + NO interaction on the $MnCe/Al_2O_3$ sample are presented in Fig. 10. Comparison with Fig. 4 suggests that here even at low temperatures carbonate-like structures are formed. However, because of the complexity of the spectra

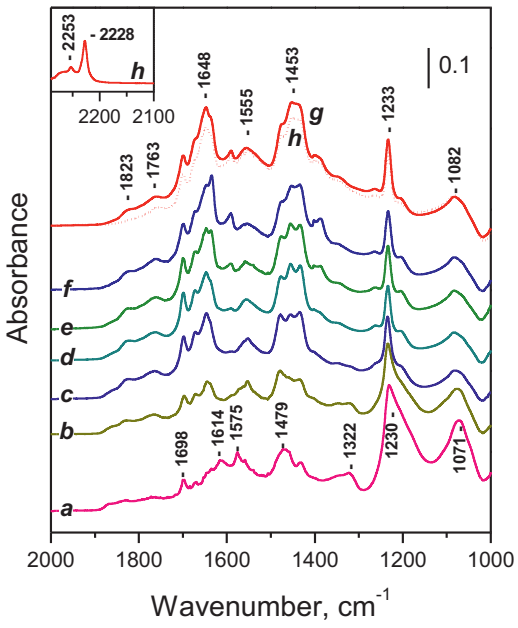

Fig. 9. FTIR spectra of the surface species produced after interaction of NO and CO (1 kPa initial equilibrium pressure of each gas) with Mn/Al_2O_3. Temperature of interaction 373 (a), 423 (b), 473 (c), 523 (d), 573 (e), 623 (f) and 673 K (g) and after evacuation (h). The spectra are background and gas-phase corrected.

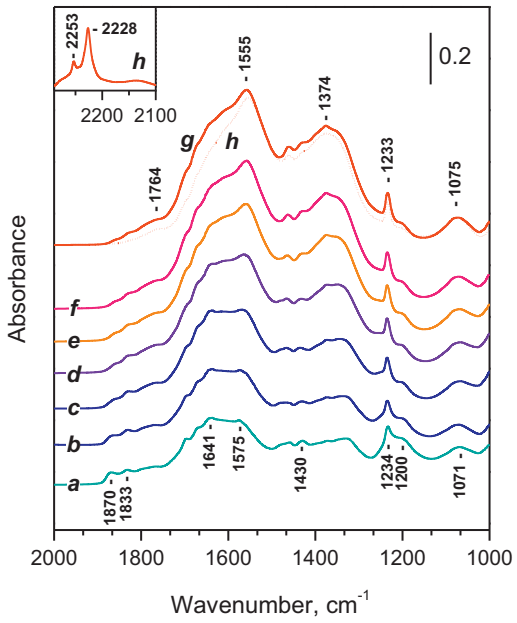

Fig. 10. FTIR spectra of the surface species produced after interaction of NO and CO (1 kPa initial equilibrium pressure of each gas) with $MnCe/Al_2O_3$. Temperature of interaction 373 (a), 423 (b), 473 (c), 523 (d), 573 (e), 623 (f) and 673 K (g) and after evacuation (h). The spectra are background and gas-phase corrected.

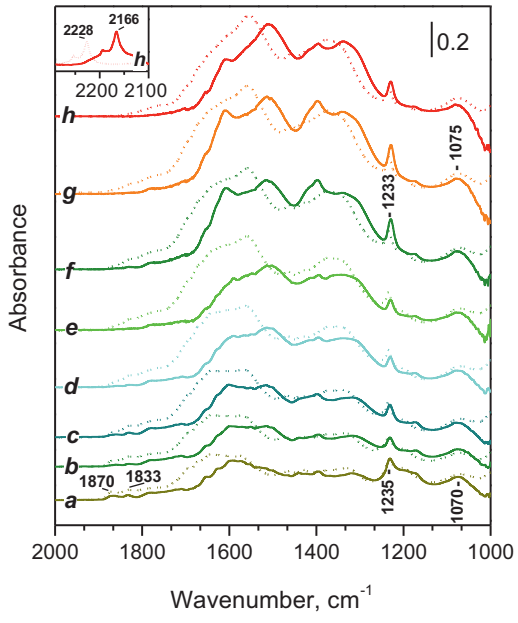

Fig. 11. FTIR spectra of the surface species produced after interaction of NO and ^{13}CO (1 kPa initial equilibrium pressure of each gas) with $MnCe/Al_2O_3$. Temperature of interaction 373 (a), 423 (b), 473 (c), 523 (d), 573 (e), 623 (f) and 673 K (g) and after evacuation (h). The corresponding spectra registered using ^{12}CO are presented by dotted lines. The spectra are background and gas-phase corrected.

it is not so easy to draw definite conclusions on the existence of nitrogen-oxo species. This will be done when discussing the spectra of coadsorbed $^{13}CO + NO$. Note that the band at 2253 cm^{-1} (already attributed to Mn–NCO species) appeared with enhanced intensity.

In this case the band assigned to adsorbed CO_2 was of high intensity and increased with the interaction temperature (Fig. S9 from the Supplementary Content, spectra d–g).

3.2.5. Experiments involving ^{13}CO

In order to distinguish unambiguously the carbon- and nitrogen-containing oxo-species formed during CO and NO interaction on the $MnCe/Al_2O_3$ sample, we have studied coadsorption of ^{13}CO and NO. The resulting spectra are presented in Fig. 11. For comparison, the analogous spectra registered with ^{12}CO are shown with dotted lines.

Let us first analyze the spectra in the 2300–2100 cm^{-1} region (see the inset in Fig. 11). The band at 2253 and 2228 cm^{-1} (registered after CO + NO coadsorption) are observed at 2194 and 2166 cm^{-1}, respectively, when ^{13}CO was used in the experiments. Therefore, the isotopic shift factor in these cases is 0.9735–0.9738. Although the isotopic shift factor of the broad band at 2176 cm^{-1} cannot be calculated exactly because of superimposition, it is similar. The observed factors are lower from both, the ^{12}CO–^{13}CO (0.97777) and ^{12}CN–^{13}CN (0.97907) theoretically expected isotopic shift factors. However, considering isocyanates as pseudo-diatomic molecules should result in a smaller shift factor (0.8516). Because the pseudo-diatomic model is a border one, we can stress that the results indicate the species under consideration are indeed isocyanates.

Consider now the lower frequency region. It was reported that the bending modes of the hydrogencarbonate OH groups around 1235 cm^{-1} are very slightly affected by the ^{12}C–^{13}C substitution [39]. Indeed, they were shifted by only 5–6 cm^{-1} in our experiments. Similar effect was reported [39] and observed here for the modes around 1070 cm^{-1}. Considering the other bands, it is seen that in all cases they are shifted by a factor similar to 0.97777 (^{12}CO–^{13}CO isotopic shift factor). This is valid for the whole temperature region, i.e. with this sample, even after CO + NO interaction at 373 K, carbonate-like species dominate on the surface.

3.3. Catalytic performance

The catalytic properties of the samples were tested in three reactions of environmental interest: CO oxidation, direct NO decomposition and CO + NO reaction.

3.3.1. CO oxidation

The catalytic behavior of the samples in the oxidation of CO by O_2 is compared in Fig. 12. The samples show different activities increasing with temperature and no full conversion was achieved even at 773 K. As expected, the lowest activity was demonstrated by the alumina support with no conversion even at 373 K. The samples Ce/Al_2O_3 and Mn/Al_2O_3 possessed similar conversion degrees in the low (up to 423 K) and in high (673–773 K)

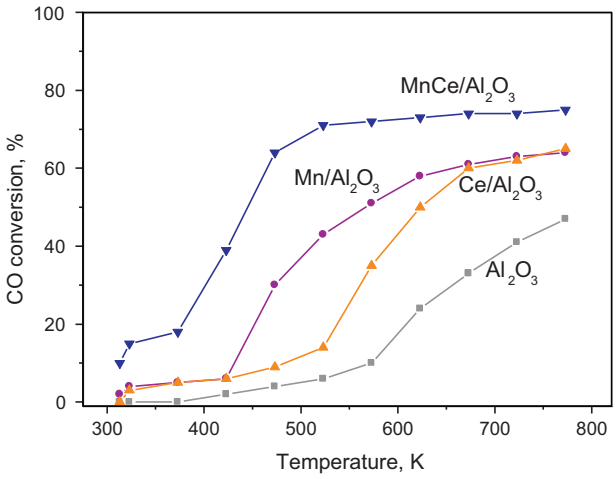

Fig. 12. Temperature dependence of CO oxidation for Al_2O_3, Mn/Al_2O_3, Ce/Al_2O_3 and $MnCe/Al_2O_3$.

temperature regions. However, they differed in the middle temperature interval (423–673 K), where the conversion degree of CO for Mn/Al_2O_3 exceeded this for Ce/Al_2O_3 (the light-off temperatures are T_{50} = 573 K and T_{50} = 623 K respectively). The highest activity was demonstrated by the bimetallic $MnCe/Al_2O_3$ catalysts reaching a conversion of ca. 70% at 523 K and a light-off temperature of 443 K.

The temperature dependence for the $MnCe/Al_2O_3$ sample is not typical for CO conversion. From one side the relatively low activity at high temperatures could be explained by the concurrent proceeding of the water gas shift reaction. Indeed, we have established such effect, but it is limited to ca. 2% from the low residual water concentration (150 ppm). However, decrease of the flow rate resulted in increase of the CO conversion up to 98% (Fig. S10 from the Supplementary Content). Therefore, the relatively low activities of the $MnCe/Al_2O_3$ sample at high temperatures are associated with the high flow rate in these experiments.

More information on the reaction mechanism could be gained by examining the desorption picture of CO, O_2 and CO_2 after each steady stage measuring temperature (Table S1 from the Supplementary Content). As could be seen the desorption products from the two samples are completely different. For Ce/Al_2O_3 we detected desorption of significant amounts of CO and O_2. This is expected as it was found that addition of CeO_2 can not only promote the adsorption of O_2 and the reaction of adsorbed CO with surface oxygen species to form CO_2, but also increases the CO_2 desorption speed [46]. The oxidation of CO on this catalyst proceeds between adsorbed CO and O_2 on the surface. No desorption of CO_2 was seen, evidencing the fast release of the product. The isothermal desorption data for Mn/Al_2O_3 shows no desorption for all three gases. This suggests fast adsorption of the reagents and desorption of the product. The desorption measurements of the alumina support show desorption of CO and CO_2 for all temperatures and desorption of O_2 at temperatures up to 573 K.

The light-off for the bimetallic $MnCe/Al_2O_3$ is much lower (T_{50} = 443 K) as compared to the other samples. The high activity of the bi-component supported catalyst indicates a cooperative effect of Mn and Ce in the CO oxidation. This is well demonstrated by the twofold increase in the specific activity at 473 K for $MnCe/Al_2O_3$ (1.92 h^{-1}) as compared to the values for Mn/Al_2O_3 (0.9 h^{-1}) and Ce/Al_2O_3 (0.27 h^{-1}). The desorption spectra of CO, CO_2 and O_2 are similar to Ce/Al_2O_3 up to 573 K and to Mn/Al_2O_3 at higher temperatures. A comparison with the FTIR spectra indicates that the activity of the catalysts correlates well with their ability to form carbonate-like structures. Imamura et al. [47] found that even small addition of cerium remarkably affect the activity of manganese catalysts in the oxidation of CO by providing oxygen to manganese oxide thus easily changing its oxidation state. Our results indicate that another important role of ceria is keeping manganese highly dispersed thus ensuring a high concentration of catalytically active sites.

3.3.2. NO decomposition

The activities of the catalysts in NO decomposition are quite lower as compared to CO oxidation activities (Fig. 13). For all samples the activity increases monotonically with the temperature. The most efficient (bi-metallic) catalyst reaches just 15% NO conversion at 773 K. The order of activity is $Al_2O_3 < Ce/Al_2O_3 < Mn/Al_2O_3 < MnCe/Al_2O_3$. The specific activities for all catalysts do not show considerable promotion effect of Mn and Ce in the bi-metallic sample (at 673 K the values are 0.26 h^{-1} for Ce/Al_2O_3, 0.29 h^{-1} for Mn/Al_2O_3 and 0.39 h^{-1} for $MnCe/Al_2O_3$).

The desorption data for the studied catalysts are given in Table S2 from the Supplementary Content. The data for the alumina support indicate NO desorption up to 523 K and O_2 desorption above 573 K. No desorption of N_2 was detected in the whole temperature interval. For all temperatures desorption of N_2O, decreasing with temperature, was observed. This is indicative for two-step decomposition reaction via formation of N_2O intermediate.

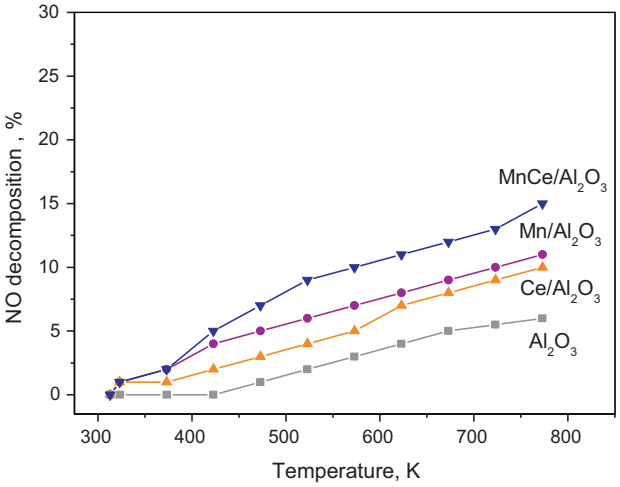

Fig. 13. Temperature dependence of NO decomposition for Al_2O_3, Mn/Al_2O_3, Ce/Al_2O_3 and $MnCe/Al_2O_3$.

The desorption patterns of Mn/Al_2O_3 at temperatures up to 523 K show NO, N_2O, N_2 and O_2 as products. No desorption of NO was detected above 623 K and the rate controlling step is the desorption of the products (N_2O, N_2 and O_2).

The desorption patterns of Ce/Al_2O_3 show desorption of NO, N_2 and O_2 at temperatures up to 623 K and N_2O at all temperatures.

The picture with the sample $MnCe/Al_2O_3$ is more complex. It could be considered as a non linear combination of the desorption patterns of the mono-component samples. At low temperatures (523 K) the results are similar to those obtained with Mn/Al_2O_3 and desorption of NO, N_2O, N_2 and O_2 is observed. At higher temperatures (above 523 K) only N_2O desorption decreasing with temperature along with the O_2 desorption increasing with temperature are registered. At the end of the temperature interval no N_2O is observed. It could be noted that with increasing the temperature the N_2 selectivity increases but the N_2O content remains almost same. For all catalysts Ce/Al_2O_3, Mn/Al_2O_3 and $MnCe/Al_2O_3$ a two-step NO decomposition process by Langmuir–Hinshelwood mechanism is probable.

Comparison of the catalytic results with the IR spectra does not show any correlation between the activity and particular surface species. This indicates that the species we have observed are spectator. Therefore, in this case we are not able to draw any FTIR-based mechanistic conclusions.

3.3.3. NO + CO interaction

Fig. 14 presents the temperature dependence of the conversion degree for NO and CO on the catalysts studied. Overall, alumina demonstrates the lowest activity, followed by Mn/Al_2O_3 and Ce/Al_2O_3 catalysts, while $MnCe/Al_2O_3$ was characterized by the highest activity. It is to be noted that the conversion curves of CO and NO on Al_2O_3 are similar which indicates that NO + CO is the dominant reaction. The same situation was observed with the Mn/Al_2O_3 and Ce/Al_2O_3 catalysts. With the bimetallic sample the conversion of NO in the low temperature region (298–373 K) exceeds the CO conversion. This could be explained by proceeding of reactive NO adsorption at these conditions.

We could notice a good activity in the reaction and a high selectivity for N_2 formation below 473 K, although formation of some N_2O is also registered. When the temperature was higher, no N_2O was measured and the reaction proceeds mainly to N_2, NO_2 and CO_2. Kapteijn et al. [48] also found that alumina supported

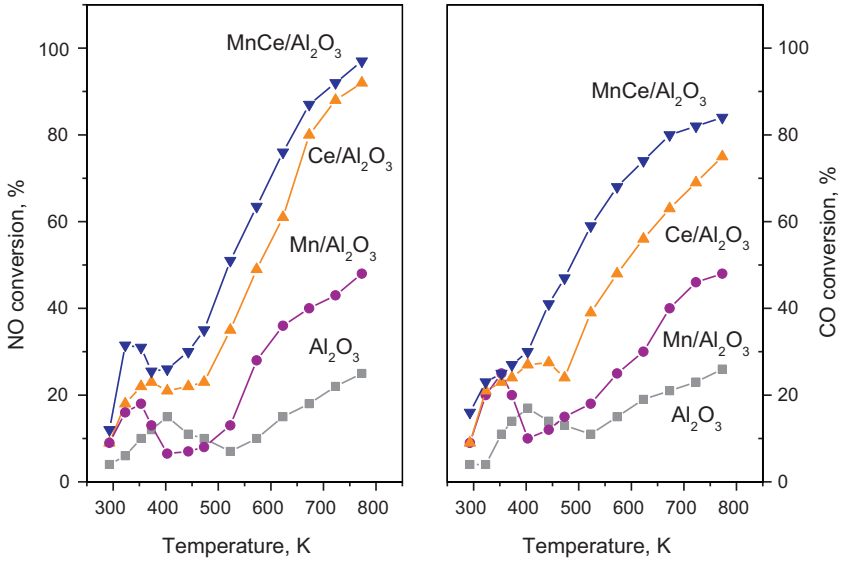

Fig. 14. Temperature dependence of NO reduction with CO for $MnCe/Al_2O_3$, Mn/Al_2O_3, Ce/Al_2O_3 and Al_2O_3.

manganese oxides exhibited a high selectivity for N_2 formation below 425 K. The amount of N_2O formed decreased with temperature [48] and manganese loading [49]. It has been suggested that N_2O formation occurred mostly on well-ordered manganese oxide crystalline planes because of the presence of highly reactive oxygen.

Pure Al_2O_3 support shows low activity of about 25% even at 773 K. The conversion curves pass through a local maximum at around 400 K and minimum at ca. 523 K. Comparison with the FTIR results allows associating the maximum at 400 K with NO-precovered surface. At higher temperatures the predominant surface species are carbonate-like structures which reflect in lowering the catalyst activity.

A similar picture was observed with the Mn/Al_2O_3 catalyst. However, the local maximum and the minimum are considerably shifted to lower temperatures, ca. 350 and 400 K, respectively. As a result, the catalytic activity of Mn/Al_2O_3 is higher than that of the pure support only at temperatures below 400 K and above 523 K. Here again, the local maximum correlates well with the FTIR observations: it was found that the carbonate-like structures becomes more important on this sample at lower temperatures, as compared to the support.

The Ce/Al_2O_3 catalyst is considerably more active than Al_2O_3 in the whole temperature interval. The local maxima for NO and CO conversion do not coincide but are at higher temperatures as compared to the Mn/Al_2O_3 sample. At temperatures above 523 K the NO conversion degree is greater than this for CO, suggesting that on the surface of this catalyst a secondary reaction of NO decomposition proceeds in addition to the reduction of NO.

The alumina supported bi-metallic catalyst shows highest catalytic activity; its light-off temperature for NO is T_{50} = 493 K and for CO, T_{50} = 483 K. These parameters are T_{50} = 773 K for both reagents with the Mn/Al_2O_3 and T_{50} = 573 K for NO and T_{50} = 623 K for CO with the Ce/Al_2O_3 sample, respectively. The desorption picture for $MnCe/Al_2O_3$ shows clear release of NO, CO, N_2 and CO_2 above 313 K. With increasing temperature the quantity of NO desorbed decreases and this for CO increases up to 523 K, where no NO is evolved.

In this case no clear maximum was detected in the CO conversion curve which is consistent with the IR observation that the surface of this catalyst is precovered mainly by carbonates even at low temperatures. However, local maximum was observed for NO conversions. This indicates that, in addition to CO + NO interaction, at low temperatures NO decomposition also occurs.

4. Conclusions

The objectives of this study were to investigate the surface chemistry of three catalysts: Ce/Al_2O_3, Mn/Al_2O_3 and $MnCe/Al_2O_3$ in order to obtain more information on the mechanism of reaction of environmental interests, such as CO oxidation, NO decomposition and CO + NO interaction. It was established that:

- Manganese is better dispersed and is in a lower average oxidation state on $MnCe/Al_2O_3$ catalyst as compared to Mn/Al_2O_3.
- Mn and Ce species deposited on alumina by impregnation are located at (i) part of the sites where OH groups have originally existed on the support and (ii) part of the Lewis acid-basic pairs on alumina.
- Low-temperature CO adsorption on Al_2O_3 results in formation of two carbonyl bands: Al^{3+}–CO at 2200 cm^{-1} (shifting to 2185 cm^{-1} with coverage increase) and OH–CO at 2157 cm^{-1}. These bands are registered with reduced intensity with the supported samples. In addition, carbonyls associated with Mn and Ce cation are observed with the supported samples in the 2180–2170 cm^{-1} region, i.e. CO is appropriate probe for detection but not to distinguishing between Mn and Ce sites in this case.
- Interaction of all samples with CO at $T \geq 373$ K leads to formation of carbonates and hydrogencarbonates which amount increases with the temperature of interaction (373–673 K) and in the sequence $Al_2O_3 < Ce/Al_2O_3 < Mn/Al_2O_3 \ll MnCe/Al_2O_3$.
- Interaction of all samples with NO at $T \geq 373$ K leads to formation of different nitrogen oxo-compounds and, with the Mn/Al_2O_3 and $MnCe/Al_2O_3$ samples, to manganese nitrosyls (1873, 1833 and 1787 cm^{-1}). The latter are in much higher amount with the $MnCe/Al_2O_3$ sample. The fact that NO forms nitrosyls with manganese cations but not with aluminum and cerium sites makes this molecule a good probe for selective detection of surface manganese sites.
- Some surface carbon species on Mn/Al_2O_3 resist oxidation with O_2 even at 673 K. However, they interact with NO producing carbonates and hydrogencarbonates and can be removed by several NO adsorption–desorption cycles. Similar carbon was found on the $MnCe/Al_2O_3$ sample but in lower concentration.
- Interaction between CO and NO on the samples results in formation of isocyanates, (hydrogen)carbonates and nitrogen oxo-compounds structures. When the interaction occurs at 373 K, the surfaces of the Al_2O_3, Ce/Al_2O_3 and Mn/Al_2O_3 are

covered mainly by NO_x species. With increase of the interaction temperature these species are gradually replaced by (hydrogen)carbonates. The temperature of this replacement decreases in the order Al_2O_3–Ce/Al_2O_3–Mn/Al_2O_3. With the MnCe/Al_2O_3 sample carbonates dominate even at 373 K interaction.

- The samples show different behavior in catalytic reactions of environmental interest: CO oxidation, NO decomposition and NO + CO interaction. The NO + CO interaction occurs in two regimes which are associated with NO_x- (low temperature) and (hydrogen)carbonate-precovered surfaces (high temperature). In all cases the bimetallic MnCe/Al_2O_3 sample manifest highest catalytic activity.

Acknowledgment

The authors are indebted to the National Science Fund of Bulgaria (Contract DTK 02/64/2009 and DCVP 02/2/2009).

Appendix A. Supplementary data

Supplementary data associated with this article can be found, in the online version, at http://dx.doi.org/10.1016/j.apcatb.2013.03.012.

References

[1] I. Pârvulescu, P. Grange, B. Delmon, Catalysis Today 46 (1998) 233–316.
[2] M. Shelef, Chemical Reviews 95 (1995) 209–225.
[3] N. Imanaka, T. Masui, Applied Catalysis A: General 431/432 (2012) 1–8.
[4] N. Le Phuc, X. Courtois, F. Can, S. Royer, P. Marecot, D. Duprez, Applied Catalysis B: Environmental 102 (2011) 362–371.
[5] S. Royer, D. Duprez, ChemCatChem 3 (2011) 24–65.
[6] Tz. Venkov, Hr. Klimev, M.A. Centeno, J.A. Odriozola, K. Hadjiivanov, Catalysis Communications 7 (2006) 308–313.
[7] W. Liu, M. Flytzanistephanopoulos, Journal of Catalysis 153 (1995) 317–332.
[8] G. Busca, M. Larruba, L. Arrighi, G. Ramis, Catalysis Today 107/108 (2005) 139–148.
[9] T. Weingang, S. Kuba, K. Hadjiivanov, H. Knözinger, Journal of Catalysis 209 (2002) 539–546.
[10] R. Burch, J.P. Breen, F.C. Meunier, Applied Catalysis B: Environmental 39 (2002) 283–303.
[11] J. Chen, Y. Zhan, J. Zhu, C. Chen, X. Lin, Q. Zheng, Applied Catalysis A: General 377 (2010) 121–127.
[12] C. Hardacre, R.M. Ormerod, R.M. Lambert, Journal of Physical Chemistry 98 (1994) 10901–10905.
[13] Z. Lendzion-Bielun, M.M. Betahar, S. Monteverdi, D. Moszynski, U. Narkievicz, Catalysis Letters 134 (2010) 196–203.
[14] M. Machida, M. Uto, D. Kurogi, T. Kijima, Chemistry of Materials 12 (2000) 3158–3164.
[15] M. Machida, D. Kurogi, T. Kijima, Catalysis Today 84 (2003) 201–207.
[16] J.-W. Park, J.-H. Jeong, W.-L. Yoon, H. Jung, H.-T. Lee, D.-K. Lee, Y.-K. Park, Y.-W. Rhee, Applied Catalysis A: General 274 (2004) 25–32.
[17] I. Spassova, T. Tsontcheva, N. Velichkova, M. Khristova, D. Nihtianova, Journal of Colloid and Interface Science 374 (2012) 267–277.
[18] A. Bensalem, F. Bozon-Verduraz, M. Delamar, G. Bugli, Applied Catalysis 121 (1995) 81–93.
[19] A. Bensalem, J.C. Muller, F. Bozon-Verduraz, Journal of the Chemical Society, Faraday Transactions 88 (1992) 153–154.
[20] M. Raciulete, P. Afanasiev, Applied Catalysis A: General 368 (2009) 79–86.
[21] J. Boyero Macstre, E. Fernandez Lopez, J.M. Gallardo-Amores, R. Ruano Casero, V. Sanchez Escribano, E. Perez Berna, International Journal of Inorganic Materials 3 (2001) 889–899.
[22] H. Knözinger, P. Ratnasamy, Catalysis Reviews: Science and Engineering 17 (1978) 31–70.
[23] G. Della Gatta, B. Fubini, G. Ghiotti, C. Morterra, Journal of Catalysis 43 (1976) 90–98.
[24] K. Góra-Marek, M. Derewiński, P. Sarv, J. Datka, Catalysis Today 101 (2005) 131–138.
[25] B. Bonelli, P. Palmero, F. Lomello, M. Armandi, M. Lombardi, Journal of Materials Science 45 (2010) 6115–6125.
[26] W. El-Nadjar, M. Bonne, E. Trela, L. Rouleau, A. Mino, S. Hocine, E. Payen, C. Lancelot, C. Lamonier, P. Blanchard, X. Courtois, F. Can, D. Duprez, S. Royer, Microporous and Mesoporous Materials 158 (2012) 88–98.
[27] Tz. Venkov, K. Hadjiivanov, D. Klissurski, Physical Chemistry Chemical Physics 4 (2002) 2443–2448.
[28] T.H. Ballinger, J.T. Yates Jr., Langmuir 7 (1991) 3041–3045.
[29] A.A. Tsyganenko, V.N. Filimonov, Journal of Molecular Structure 19 (1973) 579–589.
[30] G. Busca, V. Lorenzelli, Materials Chemistry 7 (1982) 89–126.
[31] A.A. Davydov, Infrared Spectroscopy of Adsorbed Species on the Surface of Transition Metal Oxides, Wiley, Chichester, 1990.
[32] C. Binet, M. Daturi, J.C. Lavalley, Catalysis Today 50 (1999) 207–225; J. Baltrusaitis, J. Schuttlefield, E. Zeitler, V.H. Grassian, Chemical Engineering Journal 170 (2011) 471–481.
[33] K. Hadjiivanov, G. Vayssilov, Advances in Catalysis 47 (2002) 307–511.
[34] K. Khadzhiivanov, A. Davydov, Kinetika i Kataliz 29 (1988) 398–402.
[35] K. Hadjiivanov, D. Klissurski, M. Kantcheva, A. Davydov, Journal of the Chemical Society, Faraday Transactions 87 (1991) 907–911.
[36] M. Zaki, H. Knözinger, Materials Chemistry and Physics 17 (1987) 201–215.
[37] R. Soltanov, E. Paukshtis, E. Yurchenko, Kinetika i Kataliz 23 (1982) 135–141.
[38] K. Nakamoto, Infrared Spectra and Raman of Inorganic and Coordination Compounds, 4th ed., Wiley, New York, 1986.
[39] G.N. Vayssilov, M. Mihaylov, P. St. Petkov, K.I. Hadjiivanov, K.M. Neyman, Journal of Physical Chemistry C 115 (2011) 23435–23454.
[40] K. Hadjiivanov, Catalysis Reviews: Science and Engineering 42 (2000) 71–144.
[41] K. Hadjiivanov, Catalysis Letters 68 (2000) 157–161.
[42] F. Kapteijn, L. Singoredjo, M. van Drill, A. Andreini, J. Moulijn, G. Ramis, G. Busca, Journal of Catalysis 150 (1994) 105–116.
[43] M. Kantcheva, Journal of Catalysis 204 (2001) 479–494.
[44] A. Aylor, L. Lobree, J. Reimer, A.T. Bell, Journal of Catalysis 170 (1997) 390–401.
[45] G. Bamwenda, A. Obuchi, A. Ogata, K. Mizuno, Chemistry Letters 23 (1994) 2109–2112.
[46] J. Li, G. Lu, G. Wu, D. Mao, Y. Wang, Y. Guo, Catalysis Science & Technology 2 (2012) 1865–1871.
[47] S. Imamura, M. Shono, N. Okamoto, A. Hamada, S. Ishida, Applied Catalysis A: General 142 (1996) 279–288.
[48] L. Singoredjo, F. Kapteijn, Studies in Surface Science and Catalysis 75C (1993) 2705–2708.
[49] S. Hodjati, K. Vaezzadeh, C. Petit, V. Pitchon, A. Kiennemann, Applied Catalysis B: Environmental 26 (2000) 5–16.